

# Moving Object Captured with Pink Noise Pattern in Computational Ghost Imaging

Xiaoyu Nie,<sup>1,2</sup> Xingchen Zhao,<sup>1</sup> Tao Peng,<sup>1,\*</sup> and Marlan O. Scully<sup>1,3</sup>

<sup>1</sup>*Department of Physics and Astronomy, Texas A&M University, College Station, Texas, 77843, USA*

<sup>2</sup>*Physics Department, Xi'an Jiaotong University, Xi'an, Shaanxi 710049, China*

<sup>3</sup>*Baylor Research and Innovation Collaborative, Baylor University, Waco, 76706, USA*

(Dated: May 18, 2022)

We develop and experimentally demonstrate an imaging method based on the pink noise pattern in the computational ghost imaging (CGI) system, which has a strong ability to photograph moving objects. To examine its unique ability and scope of application, the object oscillates with variable amplitude in horizontal axis, and the result via commonly used white noise are also measured as a comparison. We show that our method can image the object when the white noise method fails. In addition, our method uses less number of patterns, and enhances the signal-to-noise ratio (SNR) to a great extent.

## I. INTRODUCTION

Ghost imaging (GI) [1–3], a practice with single-pixel imaging, possesses advanced features comparing to the conventional photographing. The thermal light GI method is immune to atmosphere turbulence [4], and can achieve high imaging resolution [5–7]. To further ameliorate and simplify the system, computational ghost imaging (CGI) [8, 9] is invented, where the reference beam is alternated by loading pre-generated patterns in computer memories onto the Digital Micro-mirror Devices (DMD). Thus, CGI uses a single element detector to reconstruct images by sequentially recording the correlation between a set of intensity and their corresponding patterns, which has non-conventional applications such as wide spectrum imaging [10, 11], depth mapping [12], X-ray imaging [13], and remote sensing [14].

However, unlike conventional photographing which only need to take one photo for objects, CGI requires a large number of samplings to reconstruct an high quality image. The minimum number of sampling is proportionate to the total number of pixels projecting on objects, in other words, the whole number of pixels within the reconstructed image [15]. Therefore, the image could be blurred or even destroyed if the target is moving. Previously, many schemes have been proposed to improve the speed of CGI [16–19] and increase the number of sampling [20, 21], while these two ways meet some paradoxes. It should be noted that if we speed up sampling to avoid big displacement of the target, the frame-rate will become higher corresponding to shorter exposure time, leading to stronger background noise from the detector and environment. Similarly, when the total number of sampling is increased, the reconstruction time will be extended, which betrays the aim of restricting the target's displacement. On the other hand, a high-precision tracking and aiming system has been proposed [22–26]. In this case, however, motion information of the object are usually required in advance, or this makes the imaging system complicated and expensive if we apply auto-tracking devices with high-precision.

In fact, in the process of moving objects reconstruction, it is nearly impossible for us to achieve a clear image of the object same as static status. Thus, obtaining its shape and enhancing the visibility should be the primary goal. From another point of view, we can equate the shooting of moving objects to the overlap of sampling static objects with a limited number of patterns. When the target moves too fast, the equivalent static sampling number will drop to fairly low so that the image quality will be destroyed, especially its signal-to-noise ratio (SNR) [15]. Recently, we developed a method to generate the so-called pink noise speckle pattern for CGI by customizing the power spectrum density of the speckle patterns [27]. Unlike white noise, the CGI with pink noise is robust to a variety of noisy environments.

In this letter, we aim to minimize the necessary sampling number as well as improve the SNR. To realized this goal in CGI system, we compare the commonly used white noise patterns with pink noise patterns loaded on DMD, and further examine its unique ability and scope of applications with several groups of comparisons when the displacement range of the target changes (0mm, 0.4mm, 0.9mm, 1.8mm, 2.7mm). The experimental setup is shown in Fig. 1. A CW laser is used to illuminate the DMD. The pattern generated by the DMD is then imaged onto the CCD which is placed on the imaging surface of the lens. In our experiment, the size of the noise patterns is 216 by 392 pixels, in which the independent changeable mirrors count for 4 by 4 pixels. The DMD contains tiny pixel-mirrors each measuring  $16\ \mu\text{m} \times 16\ \mu\text{m}$ . The object ‘*Filght*’ contains totally around 2000 independent changeable pixels, and is

---

\*Electronic address: taopeng@tamu.edu

placed close to the CCD. Here, the CCD camera can be replaced by a single pixel detector while we still put it here because it would be convenient for us to see how many pixels the *Filght* moves according to the patterns projected to CCD. We conclude that the *Filght* moves 0, 2, 5, 10, 15 independent changeable pixels on the patterns projected to CCD, respectively. The speed and acceleration of *Filght* have a random number at every moment.

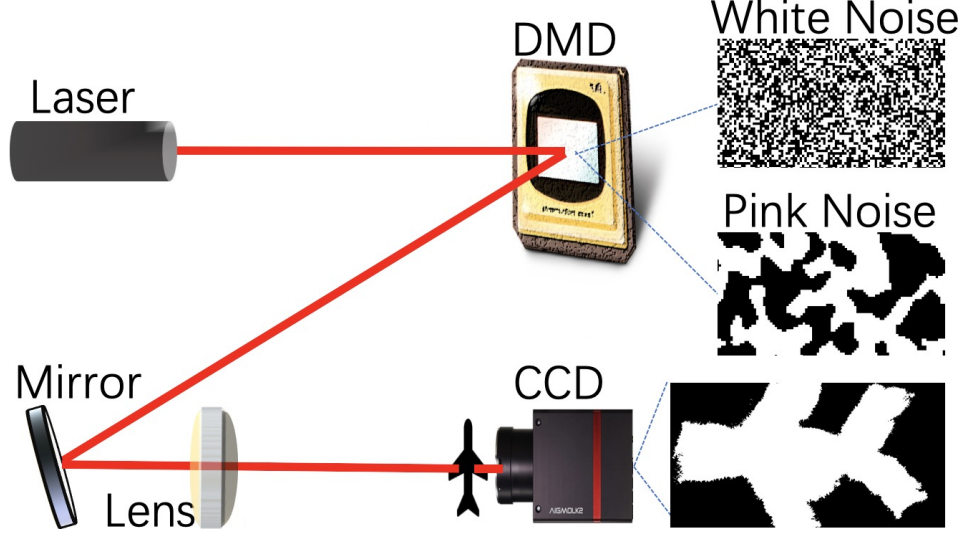


FIG. 1: Schematic of the setup for a CGI experiment. A CW laser is reflected by a DMD where the noise patterns are loaded. The reflected laser propagates to the imaging surface by a lens. The object *Filght* is put close to the CCD camera, and moves with random speed on a stage.

## II. CHARACTERISTICS OF RED NOISE

The noise patterns used in our experiment are binary pink noise patterns, in which the power of the spectrum decreases with spatial frequency. The power distribution of the spectrum is defined by  $I_{(\omega)} \sim \omega^n$ , so that for red noise patterns,  $n < 0$ . In our experiment, we set  $n = 1$ . Secondly, to make the pattern matrices real, phases applied to the power spectrum should be random conjugated symmetric. Then, we do inverse Fourier transformation on the spectrum defined above to obtain gray-scale pink noise patterns. Finally, according to their average value each pixel (127.5), we define the pixels over 127.5 to 255, while the pixels below 127.5 to 0, which will later be applied on the DMD.

We choose one pixel randomly from the pink noise patterns and calculate its auto-correlation and cross-correlation. Pink noise's spectral intensity distribution leads to a significantly positive correlation of reflectivity between pixels close to each other. This remarkable result is visibly presented in Fig. 2.

In CGI algorithms, we should collect a series of light intensity while sampling. The value of each proportionate to the transmitted pattern distribution at the sample position. In principal, light intensity collected by CCD should be  $I_i \sim \sum_x TP_i$ . We will obtain the image according to the algorithm shown in Eq. (3).

$$I_i \sim \sum_{\tilde{x}, \tilde{y}} TP_i. \quad (1)$$

Using the estimated light intensity, we get

$$\begin{aligned} R_{p \equiv (x, y)} &= \frac{\sum_i (\sum_{\tilde{x}, \tilde{y}} TP_i - \sum_{\tilde{x}, \tilde{y}} T \langle P \rangle_i) P_{i(x, y)}}{N} = \frac{\sum_{\tilde{x}, \tilde{y}} T (\sum_i P_i - \sum_i \langle P \rangle_i) P_{i(x, y)}}{N} \\ &= \sum_{\tilde{x}, \tilde{y}} T_{(\tilde{x}, \tilde{y})} \left( \frac{\sum_i P_{i(\tilde{x}, \tilde{y})} P_{i(x, y)}}{N} - \langle P \rangle_i \frac{\sum_i P_{i(x, y)}}{N} \right) = \sum_{\tilde{x}, \tilde{y}} T_{(\tilde{x}, \tilde{y})} (\langle P_{i(\tilde{x}, \tilde{y})} P_{i(x, y)} \rangle - \langle P_{i(\tilde{x}, \tilde{y})} \rangle \langle P_{i(x, y)} \rangle) \\ &= \sum_{\tilde{x}, \tilde{y}} T_{(\tilde{x}, \tilde{y})} (\langle \Delta P_{i(\tilde{x}, \tilde{y})} \Delta P_{i(x, y)} \rangle) \end{aligned} \quad (2)$$

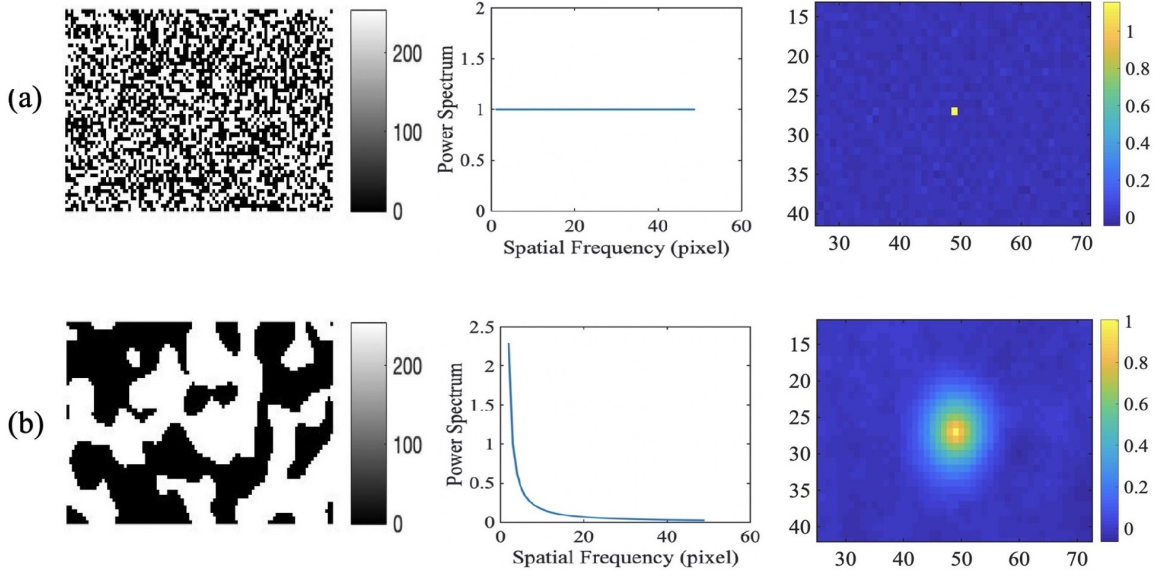


FIG. 2: From left to right: A typical pattern, one-dimensional power spectrum, and the auto-and cross-correlation of a single pixel with (a)  $n = 0$ , and (b)  $n = -1$ .

where  $T$  represents the sample transmission,  $P$  represents noise patterns,  $(\tilde{x}, \tilde{y})$  represents the coordinate on the object plane,  $(x, y)$  represents the coordinate on the DMD plane, and  $N$  is the total number of noise patterns. The  $\langle \Delta P_{i(\tilde{x}, \tilde{y})} \Delta P_{i(x, y)} \rangle$  is the cross-correlation between the pixels. For commonly used white noise or speckles in CGI, each point  $(\tilde{x}, \tilde{y})$  on the imaging plane is only contributed by the auto-correlation, thus hard to suppress the environmental noise with limited number of sampling. On the contrary, for the pink noise CGI, the intensity of every point  $(\tilde{x}, \tilde{y})$  on the imaging plane is derived by adding up both auto-correlation and cross-correlation. Here, the cross-correlation was contributed by points close to  $(\tilde{x}, \tilde{y})$ . Thus the pink noise CGI can reconstruct the image when the equivalent static sampling number drops if the target moves too fast. At the same time, the pink noise CGI can suppress the external noise and enhance the visibility which can be reflected from looking at SNR.

### III. RESULT

In the experiment, we set the distance of motion as 0 mm, 0.4 mm, 0.9 mm, 1.8 mm, and 2.7 mm, which correspond to 0, 2, 5, 10, and 15 independent pixels of noise patterns projected on the CCD surface, respectively. For each group, pink noise and white noise are applied, and the CGI results are achieved with different sampling numbers ( $N = 1000, 2000, 5000, 10000$ ). In addition, we introduce SNR to justify the quality of results. The definition of SNR is

$$SNR = \frac{\mu_{sig}}{\sigma_{sig}}. \quad (3)$$

where the  $\mu_{sig}$  is the average signal value and the  $\sigma_{sig}$  is the standard deviation of the signal.

The main results are shown in Fig. 3. The results in the first row are reconstructed images with static target. It is clear that the pink noise CGI has a much higher SNR than the white noise CGI, due to the non-zero cross-correlation from the pink noise pattern. The second row has results are achieved when the target moves with displacement = 1.8 mm. Here, identical to sampling at various position and adding them up, the equivalent total number of sampling at each position decreases significantly. Thus, the auto-correlation of the white noise is not enough to suppress environmental noise within limited number of patterns under the circumstance of moving object. On the other hand, the pink noise pattern can still give a blurry image of the object.

To further exam our method and explore the advantages of the pink noise, we also measure the target with displacement of 0.9 mm under different sample rate. The results are shown in Fig. 4. The sampling number varies from 1000 to 10000. In Fig. 4 (a-d), we can see that the shape of *Filght* could be determined by pink noise CGI even the sampling number is 1000, and becomes much clearer when  $N$  gets bigger. Nevertheless, the retrieved image from white noise CGI is totally blurred even when  $N = 10000$ . The qualities of the retrieved images are also reflected from

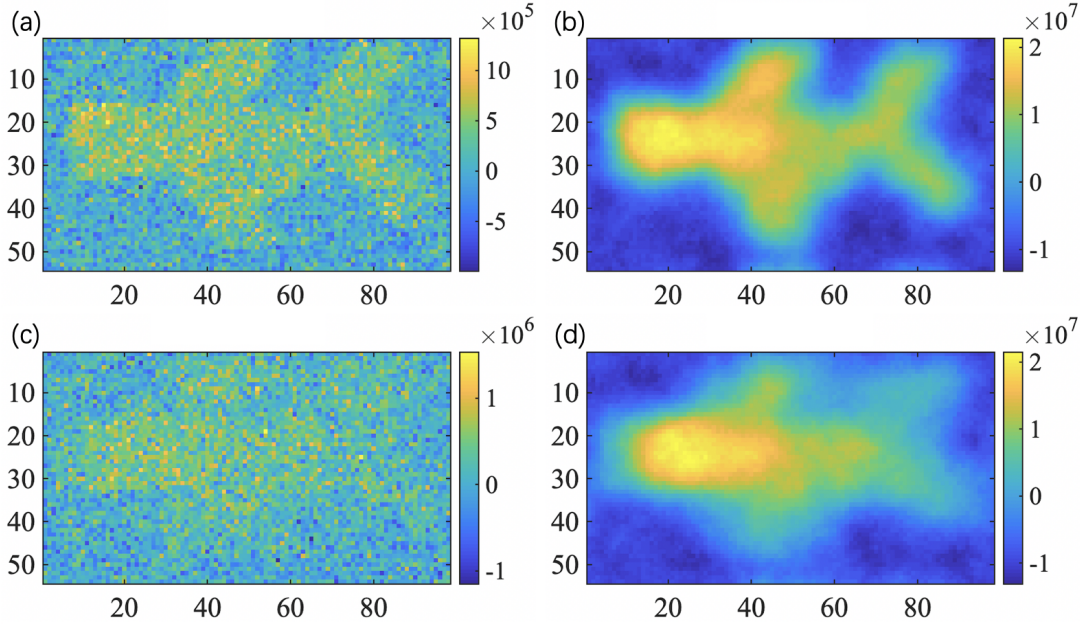


FIG. 3: The results are achieved by sampling 10000 patterns. (a) the white noise CGI result with static target. (b) the pink noise CGI result with static target. (c) the white noise CGI result with displacement = 1.8 mm. (d) the pink noise CGI result with displacement = 1.8 mm.

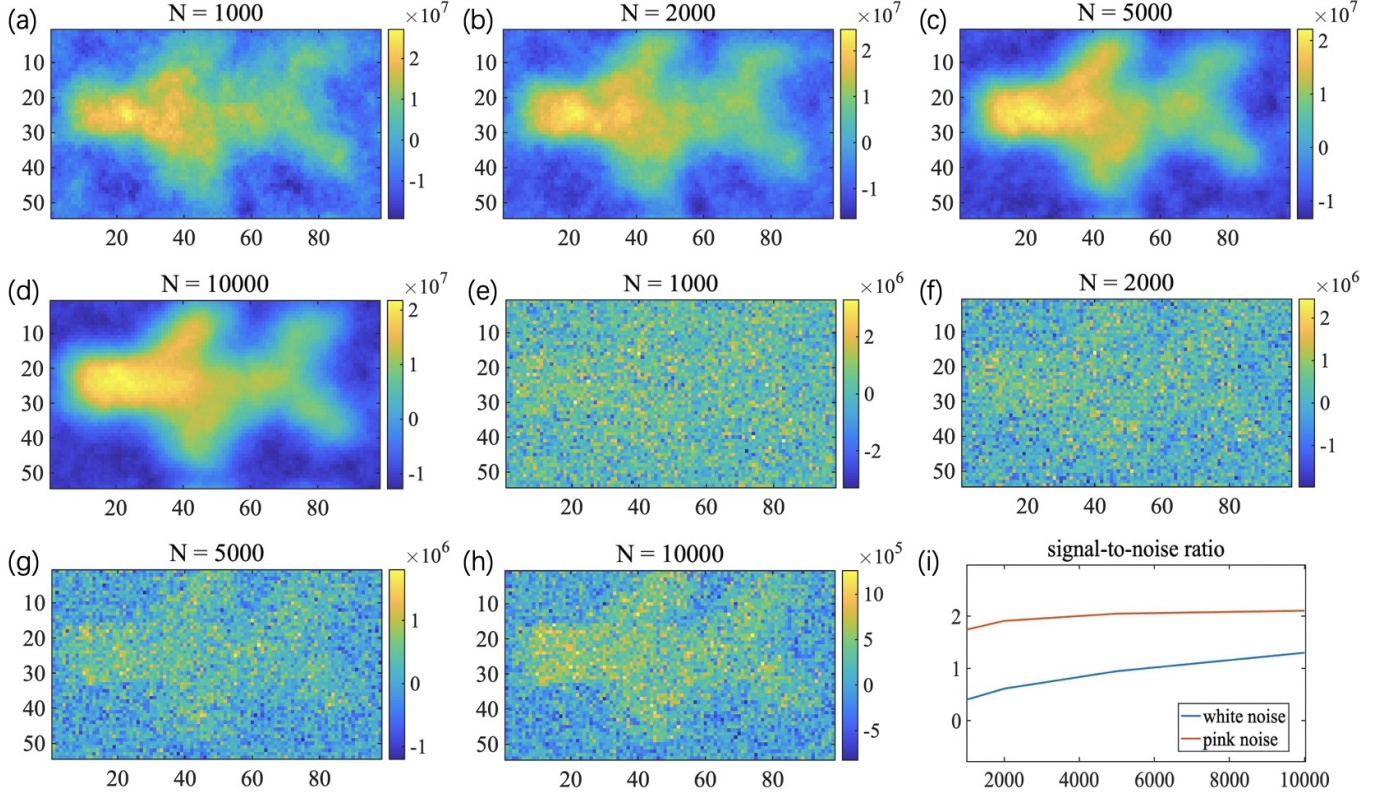


FIG. 4: Retrieved images with an object displacement of 0.9 mm. The number of sampling are shown on the title. (a)-(d): results of pink noise CGI. (e)-(h): results of white noise CGI. (i): signal to noise ratio of figure (a)-(h).

SNR (Fig. 4), in which SNR of pink noise CGI is always higher than white noise, 4 times higher when  $N = 1000$ , for instance.



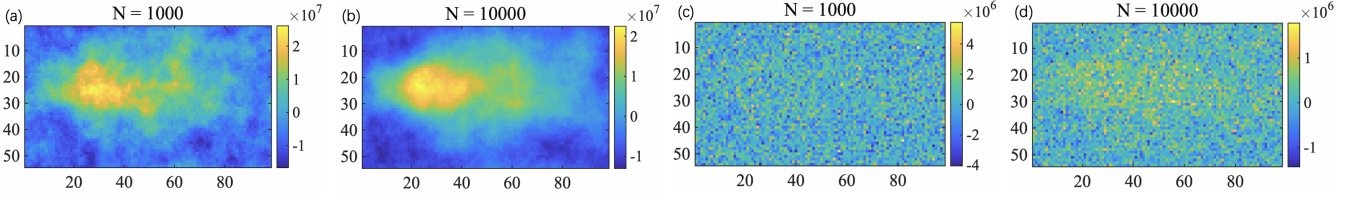


FIG. 5: Results when the displacement of the target is 2.7 mm. The number of sampling are shown on the title. (a) (b): results of pink noise CGI. (c),(d): results of white noise CGI.

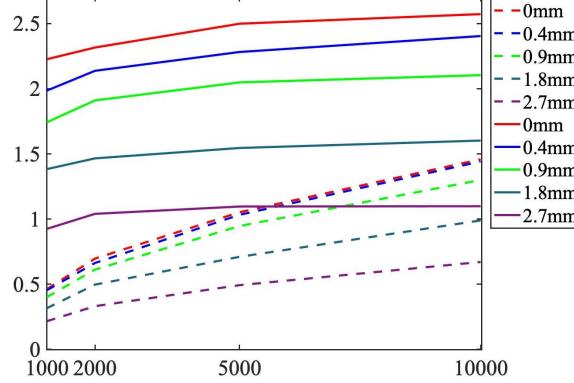


FIG. 6: SNR for different displacement. Where pink noise CGI are solid lines and white noise CGI are dashed lines.

Moreover, to explore the limits of the pink noise CGI in capturing moving object, we extend the displacement to 2.7 mm which correspond to 15 independent changeable pixels of noise patterns projected on CCD surface. It should be pointed out that the whole length of the *Flight's* arm counts for around 18 independent changeable pixels, indicating that there is almost no overlap area of arms. The results are shown in Fig. 5. The *Flight* is blurred in this situation even in pink noise CGI, but we still can extract the signal from background noise beginning in  $N = 1000$ . In white noise CGI, nothing could be achieved from  $N = 1000$  to 10000. Lastly, the SNR of all the displacements are summarized and plotted in Fig. 6. Where the solid lines are for pink noise, and dashed lines are for white noise. We see that the SNRs of pink noise are always much higher than that of the white noise with measurements done under same displacement, and when the SNRs decreases when the displacement value increases, as expected.

#### IV. CONCLUSION

In summary, we have developed a practice based on the pink noise pattern in CGI system to reconstruct images of a moving object, which is indicated by the simultaneously improved SNR and fewer sampling number. Experimentally, the SNR of pink noise CGI is usually 4 to 5 times higher than the SNR of white noise CGI especially when the sample rate is low. The major philosophy of this scheme is that it takes advantage of the positive cross-correlation which is unique of the pink noise pattern, giving the robustness of ability to overcome the environmental noise, decrease the sampling number, and further ameliorate the quality of imaging. Namely, reducing the number of patterns should be loaded on DMD directly shortening the time spent on the image reconstruction process.

In addition, with the buttress of the results offered in our work, it is possible to combine the compressive sensing with pink noise CGI, which might further decrease the total required number of sampling without losing the quality of results [28, 29]. On the other hand, due to the cross-correlation, a low level of edge's sharpness is main disadvantage of pink noise CGI. However, a future amelioration might be that this pink noise CGI system can be employed with deep learning [15, 30] to improve the sharpness of results's edges, and further decrease the total number of sampling.

#### Funding.

Air Force Office of Scientific Research (Award No. FA9550-20-1-0366 DEF), Office of Naval Research (Award No. N00014-20-1-2184), Robert A. Welch Foundation (Grant No. A-1261), National Science Foundation (Grant No.

PHY-2013771).

### Acknowledgments

X. N. thanks A. Svidzinsky for his kind help during their visit at IQSE, Texas A&M University.

### Disclosures.

The authors declare no conflicts of interest.

- 
- [1] T. B. Pittman, Y. H. Shih, D. V. Strekalov, and A. V. Sergienko, *Physical Review A* **52**, R3429 (1995).
  - [2] R. S. Bennink, S. J. Bentley, and R. W. Boyd, *Physical review letters* **89**, 113601 (2002).
  - [3] X.-H. Chen, Q. Liu, K.-H. Luo, and L.-A. Wu, *Optics letters* **34**, 695 (2009).
  - [4] R. E. Meyers, K. S. Deacon, and Y. Shih, *Applied Physics Letters* **98**, 111115 (2011).
  - [5] K. Kuplicki and K. W. C. Chan, *Optics Express* **24**, 26766 (2016).
  - [6] X.-H. Chen, F.-H. Kong, Q. Fu, S.-Y. Meng, and L.-A. Wu, *Opt Lett* **42**, 5290 (2017).
  - [7] J. Sprigg, T. Peng, and Y. Shih, *Scientific reports* **6**, 38077 (2016).
  - [8] J. H. Shapiro, *Physical Review A* **78**, 061802 (2008).
  - [9] Y. Bromberg, O. Katz, and Y. Silberberg, *Physical Review A* **79**, 053840 (2009).
  - [10] N. Radwell, K. J. Mitchell, G. M. Gibson, M. P. Edgar, R. Bowman, and M. J. Padgett, *Optica* **1**, 285 (2014).
  - [11] Z. Yang, Z. Nan, Y. Sun, and Y. Yu, *Translational Neuroscience and Clinics* (2017).
  - [12] M.-J. Sun, M. P. Edgar, G. M. Gibson, B. Sun, N. Radwell, R. Lamb, and M. J. Padgett, *Nature communications* **7**, 1 (2016).
  - [13] Y. Klein, A. Schori, I. Dolbnya, K. Sawhney, and S. Shwartz, *Optics express* **27**, 3284 (2019).
  - [14] B. I. Erkmen, *JOSA A* **29**, 782 (2012).
  - [15] M. Lyu, W. Wang, H. Wang, H. Wang, G. Li, N. Chen, and G. Situ, *Scientific Reports* **7**, 17865 (2017).
  - [16] L. Wang and S. Zhao, *Photon. Res.* **4**, 240 (2016).
  - [17] W. Gong, C. Zhao, H. Yu, M. Chen, W. Xu, and S. Han, *Scientific Reports* **6**, 26133 (2016).
  - [18] S. Jiang, X. Li, Z. Zhang, W. Jiang, Y. Wang, G. He, Y. Wang, and B. Sun, *Opt. Express* **27**, 22499 (2019).
  - [19] Z.-H. Xu, W. Chen, J. Penuelas, M. Padgett, and M.-J. Sun, *Opt. Express* **26**, 2427 (2018).
  - [20] D. B. Phillips, M. J. Sun, J. M. Taylor, M. P. Edgar, S. M. Barnett, G. M. Gibson, and M. J. Padgett, *Science Advances* (2017).
  - [21] H. Li, J. Xiong, and G. Zeng, *Optical Engineering* **50**, 1 (2011).
  - [22] X. Li, C. Deng, M. Chen, W. Gong, and S. Han, *Photon. Res.* **3**, 153 (2015).
  - [23] S. Jiao, M. Sun, Y. Gao, T. Lei, Z. Xie, and X. Yuan, *Opt. Express* **27**, 12841 (2019).
  - [24] E. Li, Z. Bo, M. Chen, W. Gong, and S. Han, *Applied Physics Letters* **104**, 251120 (2014).
  - [25] O. S. Magana-Loaiza, G. A. Howland, M. Malik, and J. C. Howell, *Applied Physics Letters* **102** (2013).
  - [26] S. Sun, J.-H. Gu, H.-Z. Lin, L. Jiang, and W.-T. Liu, *Opt. Lett.* **44**, 5594 (2019).
  - [27] X. Nie, F. Yang, X. Liu, X. Zhao, R. Nessler, Z. Li, T. Peng, M. S. Zubairy, and M. O. Scully, *arXiv preprint arXiv:2009.14390* (2020).
  - [28] O. Katz, Y. Bromberg, and Y. Silberberg, *Applied Physics Letters* **95**, 739 (2009).
  - [29] C. Yi, C. Zhengdong, F. Xiang, C. Yubao, and L. Zhenyu, *Optik - International Journal for Light and Electron Optics* (2019).
  - [30] Y. He, G. Wang, G. Dong, S. Zhu, H. Chen, A. Zhang, and Z. Xu, *Scientific Reports* **8**, 6469 (2018).